Novel Fabrication Technology for Thermoelectric Infrared Sensors Using Surface Micromachining

Philipp Raimann
Hahn-Schickard
Villingen-Schwenningen, Germany
philipp.raimann@hahn-schickard.de

Sophie Billat
Hahn-Schickard
Villingen-Schwenningen, Germany
sophie.billat@hahn-schickard.de

Irina Spies
Hahn-Schickard
Villingen-Schwenningen, Germany
irina.spies@hahn-schickard.de

Jochen Dietrich
Hahn-Schickard
Villingen-Schwenningen, Germany
jochen.dietrich@hahn-schickard.de

Daniel Hoffmann
Hahn-Schickard
Villingen-Schwenningen, Germany
daniel.hoffmann@hahn-schickard.de

Steffen Keller
Hahn-Schickard
Villingen-Schwenningen, Germany
steffen.keller@hahn-schickard.de

Alfons Dehé
Hahn-Schickard,
University of Freiburg
Villingen-Schwenningen, Germany
alfons.dehe@hahn-schickard.de

***Abstract*—In this paper a novel fabrication technology for thermoelectric infrared sensors is presented. For the first time, the thermal insulation of the absorber structure is achieved by self-assembling multilayer thermocouples. After removal of a sacrificial oxide layer by vapor hydrogen fluoride (vHF) etching, the thermocouples lift off due to residual stress gradients. This provides the necessary distance between the absorber and the substrate. Compared to state-of-the-art sensors, this implementation does not require extensive bulk processing such as grinding and cavity etching to achieve a thermally isolated absorber structure. The deflection of the realized structures has shown high agreement with an analytical model which is also presented in this paper.**

Keywords*—*surface micromachining, self-assembled devices, microelectromechanical systems, thermal insulation, vHF-etching.

I. BACKGROUND

A major contributor to the success of miniaturized thermal sensors is the evolution of MEMS processes, which enable low-cost, high-volume integrated systems with low power consumption. Recently various thermal devices have been introduced for gas [1] and flow sensing [2]. However, due to the Covid 19 pandemic, especially a high demand for thermal infrared fever detectors has been observed lately. Because of the contactless measuring principle and the attractive transducer principle, thermoelectric infrared sensors are particularly suitable for this purpose [3].

Micromachining of silicon [4] is an essential method for the fabrication of thermal MEMS and is used to achieve thermal insulation from the bulk material by creating suspended structures. This key process in the realization of thermal infrared sensors is responsible for the formation of a temperature difference [3], [5]. So far, exclusively bulk micromachining [6] has been used for the implementation of thermoelectric infrared sensors. In this approach, large parts of the substrate material are removed within defined areas below the sensor structure. For this purpose, mainly anisotropic etching processes (e.g., KOH [7], TMAH [8] or EDP [9]) are used to create a thin membrane. However, since these processes only have relatively low silicon etch rates [10] long process times are required. In recent decades, particularly surface micromachining [11] has gained in importance, as it eliminates the need for time-consuming and expensive machining processes of the substrate. Here, metals (e.g., aluminum [12], [13]), polymers [14], [15] and especially oxides [16], are used as sacrificial layers, which can be selectively removed with respect to the structural materials. So far, surface micromachining in the field of infrared sensing has been used solely for the production of micro bolometers [13], [15], [17].

In this paper, a new approach to implement a thermoelectric infrared sensor is presented. Compared to state-of-the-art thermoelectric infrared sensors, this device is fabricated using surface micromachining and vHF etching. In order to enhance the quality of the thermal insulation, mechanical stress in thin layers is exploited to deflect the sensing structure from the wafer surface.

II. TECHNOLOGY

Residual stress in thermocouples is used for the first time to distance an absorber from the substrate. While the cold end of the thermocouple is connected to the substrate via an anchor, the hot junction is thermally isolated due to the mechanical spacing (Fig. 1). The functional layers consist exclusively of polysilicon, stoichiometric silicon nitride (Si_3N_4) and aluminum. Proper sizing and the combination of compressive ($\sigma < 0$) and tensile stresses ($\sigma > 0$) of the different layers allows devices to be realized without tedious etching procedures, while still providing high thermal insulation from the bulk material caused by self-assembly.

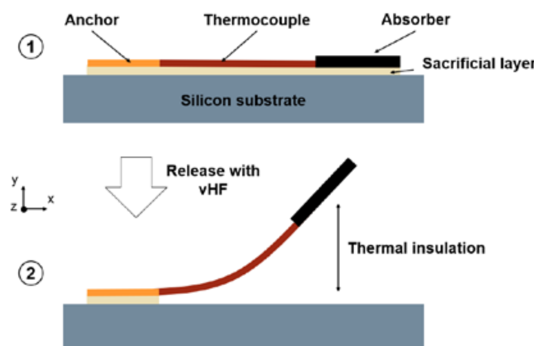

Fig. 1. Schematic of a surface micromachined thermopile IR detector.

XXX-X-XXXX-XXXX-X/XX/$XX.00 ©20XX IEEE

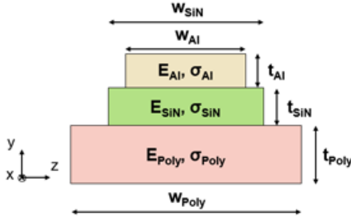

Fig. 2. Schematic of the thermocouple layer cross-section.

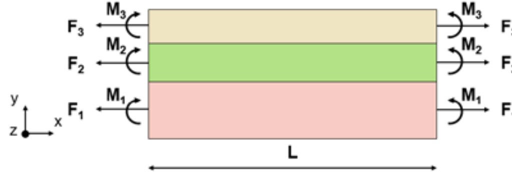

Fig. 3. Schematic of the acting forces and bending moments for deriving the mechanical deflection of the thermocouple.

TABLE I.
YOUNG'S MODULUS [31]

Material	Young's Modulus E_i (GPa)
Polysilicon	160
Si_3N_4	250
Aluminum	60

A. *Thermocouples*

In thermoelectric infrared sensors, thermocouples detect the temperature difference between the absorber and the bulk substrate [3]. In this paper, the thermocouples are realized using n-doped polysilicon and aluminum [18], [19]. The thermoelectric materials are arranged on top of each other, separated by an insulating silicon nitride to generate a stress gradient within the thermocouples (Fig. 2). The residual stress in the individual layers will be determined mainly by film thickness [20], [21], dopant concentration [22], layer composition [20], [23], [24] annealing [21], [22], reactor geometry [23] [24], process temperature and pressure, as well as the deposition rate [20] [23] [24].

B. *Absorber*

In our case the absorber elements are rectangular structures with periodically arranged circular holes. This perforation allows vHF to penetrate the holes and thus reducing the time of the sacrificial layer removal [25]. In the absorber, the optical properties of polysilicon, silicon nitride and aluminum are used to absorb the incident infrared radiation [26]. While the thermocouples are expected to bend due to the stress gradient, it is necessary to effectively minimize the mechanical deformation of the absorber. For this purpose, corrugations are introduced, which are generated by dry etching of a thermal oxide prior to the deposition of the sacrificial and functional layers.

III. MODELING OF THE MECHANICAL DEFLECTION

In this section, a model (Fig. 2 + 3) based on fundamental mechanical principles [27], [28] is introduced that can be utilized to characterize the deflection of the thermocouples.

A. *Model derivation*

After deposition, the layers i are under the influence of the initial strain ε^0_i. Assuming a linear elastic material, the strain ε^0_i in the layer can be defined by [29]:

$$\varepsilon_i^0 = \frac{\sigma_i}{E_i} \quad (1)$$

In addition, further simplifications [30] are made:

- Elimination of transverse contraction and shear stresses
- Ideal bonding of the adjacent layers
- Constant radius of curvature for all layers

The bending moment M_i of a rectangular layer cross-section in (2) can be described as a function of the unknown radius of curvature R, the Young's modulus E_i, the structure width w_i and the layer thickness t_i [29].

$$M_i = \frac{E_i w_i t_i^3}{12\,R} \quad (2)$$

Since there are no external forces acting on the structures in Fig. 3, the forces F_i and bending moments M_i in each of the individual cross sections must be in equilibrium [27], [28].

$$\sum_{i=1}^{n} F_i = 0 \quad (3)$$

$$\sum_{i=1}^{n} M_i + \sum_{i=1}^{n} F_i \left(\sum_{j=1}^{i-1} t_j + \frac{t_i}{2} \right) = 0 \quad (4)$$

In addition, continuity conditions can be used at the interfaces of the layers [27], [28].

$$\varepsilon_i^0 + \frac{F_i}{E_i t_i w_i} + \frac{t_i}{2R} = \varepsilon_{i+1}^0 + \frac{F_{i+1}}{E_{i+1} t_{i+1} w_{i+1}} - \frac{w_{i+1}}{2R} \quad (5)$$

Wolfram Mathematica 12 is finally used to solve the equations and to determine the radius of curvature R. Subsequently, geometric relationships are used in (6) to define the deflection of the thermocouple tip in x and y direction [32].

$$\Delta y = R - R\cos[L/R] \quad \text{and} \quad \Delta x = R\sin[L/R] \quad (6)$$

B. *Effect of polysilicon properties on the bending radius*

Fig. 4 presents the influence of the layer stress and the layer thickness of polysilicon on the radius of curvature prior to fabrication. Since it can be assumed that the stress within polysilicon varies with layer thickness, the bending radius can be adjusted over a wide range. This effect is exploited to achieve different deflection relative to the wafer surface.

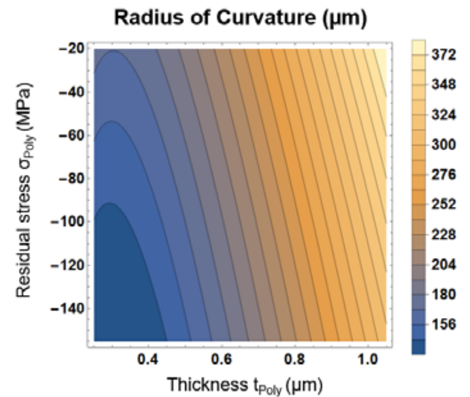

Fig. 4. Analytical modeling of the radius of curvature as a function of layer thickness and residual stress of polysilicon. (w_{Poly} = 14 µm, σ_{SiN} = 1 GPa, w_{SiN} = 12 µm, t_{SiN} = 0.2 µm, σ_{Al} = 50 MPa, w_{Al} = 8 µm, t_{Al} = 0.3 µm). The data for the Young's modulus can be taken from Table I.

IV. FABRICATION

The fabrication process of the novel thermoelectric infrared sensor starts with the growth and patterning of a 0.8 µm thick thermal oxide to optionally realize corrugations in the absorber. The sacrificial oxide layer (0.2 µm) is then deposited using a PECVD process. Afterwards, polysilicon (0.3/0.5/1.0 µm), Si_3N_4 (0.19 µm) and aluminum (0.3 µm) are deposited and patterned progressively (Table II). For the attached absorber, a size of 240x250 μm^2 was chosen.

TABLE II. STRUCTURE WIDTH OF THE MATERIALS USED FOR THERMOCOUPLES

Material	Structure Width w_i (µm)
Polysilicon	14
Si_3N_4	12
Aluminum	8

At the end, the structures are released by vHF etching using the ORBIS 3000 cluster tool from memsstar. So far, the ORBIS 3000 and the isotropic etch process has already been used in [25] to implement a micromechanical sterilization cycle counter.

V. EXPERIMENTAL RESULTS

A. Residual stress

First, the exact deposited film thickness was measured by ellipsometry, then the mechanical stress in the film was determined with a wafer geometry gauge (Table III).

TABLE III. MEASURED LAYER THICKNESS AND RESPECTIVE REDIDUAL STRESS

Material	Layer Thickness t_i (µm)	Residual Stress σ_i (MPa)
Polysilicon	0.32	-128±20
Polysilicon	0.55	-75±14
Polysilicon	1.03	-25±6
Si_3N_4	0.19	1068±20
Aluminum	not measured	37±28

As expected, the compressive stress in n-doped polysilicon revealed a decrease with increasing film thickness [20], [21]. Moreover, the stoichiometric silicon nitride could be deposited with a high tensile stress [20]. Aluminum, on the other hand, is deposited almost stress-free.

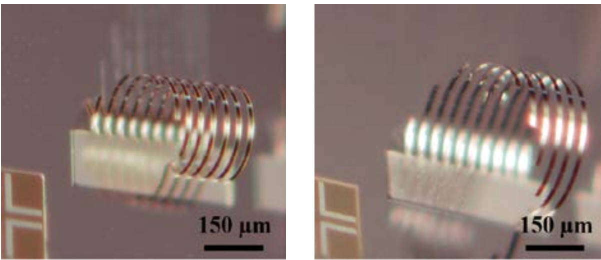

Fig. 5. Mechanical deflection of thermocouples with lengths from 100 to 1000 µm and different polysilicon layer thicknesses (left: t_{poly} = 0.32 µm; right: t_{poly} = 0.55 µm). (Note: Images captured from the side).

B. Deflection of thermocouples

After the removal of the sacrificial layer, individual thermocouples without an attached absorber deflected up to 1000 µm in length from the substrate surface. As predicted by the model, a variation of the bending radius could be obtained when using different polysilicon layer thicknesses (Fig. 5).

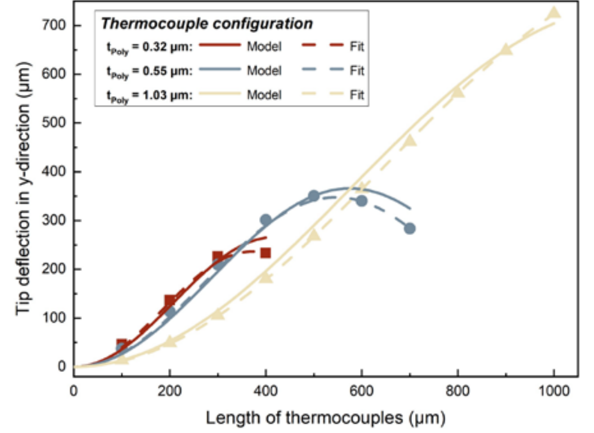

Fig. 6. Tip deflection above the wafer surface determined by optical focus variation for different polysilicon layer thicknesses as a function of thermocouple length. The measured standard deviation is in the range of the symbol dimensions. (Note: Due to the strong curvature of the structures, not all lengths of the thermocouples could be evaluated).

By using the fit function from (6), it has been shown that the deviation between the determined and modeled radius of curvature is at most about 10 %. The realized deflections of the thermocouple tips ranged from 15 to 725 µm above the substrate surface and showed deflections located on a circular arc (Fig. 6). A high reproducibility of the deflections of the structures distributed over the wafer was observed with a deviation of less than 4 % from the mean value.

C. Deflection of sensor structures

Basically, by varying the length of the thermocouples and the polysilicon layer thickness, different absorber deflections could be obtained. For thermocouples with a polysilicon layer thickness of 0.32 µm and a length of 400 µm, the attached absorber could be rotated by 180° and aligned at a height of 250 µm above the surface (Fig. 7).

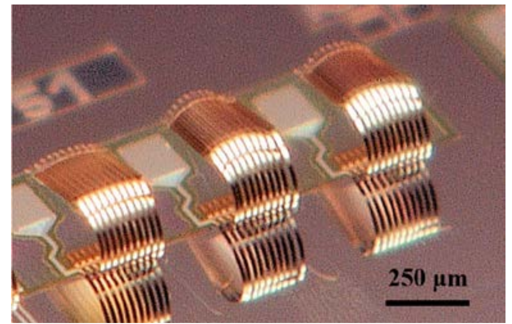

Fig. 7. Self-assembly of the sensor structures with corrugated absorber after the removal of the sacrificial layer. This distancing provides the thermal insulation. (Note: Image captured from the side).

Due to the use of corrugations in the absorber parallel to the thermocouples, the bending radius of the absorption area could be increased from 200 to 1100 µm. This made it possible to achieve nearly parallel absorber alignments above the substrate (Fig. 7 + 8).

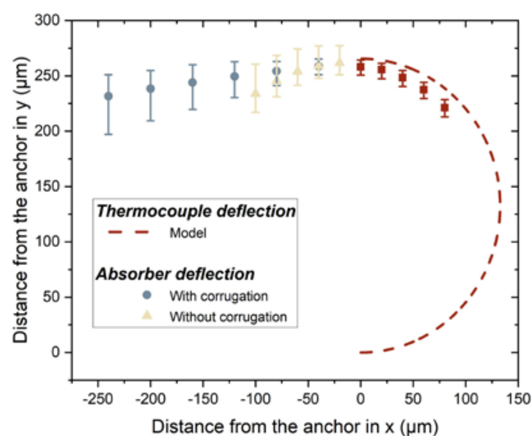

Fig. 8. Three dimensional optical scan along the sensor structures (t_{Poly} = 0.32 µm, L = 400 µm) with and without corrugations with maximum deviations. (Note: The number of measuring points is limited by the strong curvature of the structures).

VI. Conclusion and Outlook

We presented a novel fabrication process for thermoelectric infrared sensors based on surface micromachining. The thermal insulation of the absorber structure was realized by a self-assembling mechanism. The derived model demonstrated a high agreement with the measured deflections. Thermocouples with radii of curvature of 120, 175 and 415 µm could be fabricated. In addition, sensor structures with an absorber rotated by 180° could be realized at a height of 250 µm above the wafer. Further work is now focusing on thermoelectric characterization and optimization of the structures.

Acknowledgment

The ORBIS 3000 tool is funded by the University of Freiburg through the German Federal Ministry of Education and Research within the ForLab PROMYS project.

References

[1] K. Kliche, G. Kattinger, S. Billat, L. Shen, S. Messner and R. Zengerle, “Sensor for Thermal Gas Analysis Based on Micromachined Silicon-Microwires,” IEEE Sens. J., vol. 13, no. 7, pp. 2626-2635, July 2013.

[2] F. Hedrich, K. Kliche, M. Storz, S. Billat, M. Ashauer and R. Zengerle, “Thermal flow sensors for MEMS spirometric devices,” Sens. Actuators A Phys., vol. 162, no. 2, pp. 373-378, August 2010.

[3] H. Budzier and G. Gerlach, “Thermal infrared sensors: theory, optimization and practice,” John Wiley & Sons, 2011.

[4] W. Lang, “Silicon microstructuring technology,” Mater. Sci. Eng.: R: Reports, vol. 17, no. 1, pp. 1-55, September 1996.

[5] A. W. van Herwaarden, D. C. van Duyn, B. W. van Oudheusden and P. M. Sarro, “Integrated thermopile sensors,“ Sens. Actuators A Phys., vol. 22, no. 1-3, pp. 621-630, June 1990.

[6] G. T.A. Kovacs, N. I. Maluf and K. E. Petersen, “Bulk micromachining of silicon,” Proc. IEEE, vol. 86, no. 8, pp. 1536-1551, August 1998.

[7] R. Iosub, C. Moldovan and M. Modreanu, “Silicon membranes fabrication by wet anisotropic etching,” Sens. Actuators A Phys., vol. 99, no. 1-2, pp. 104-111, April 2002.

[8] O. Tabata, R. Asahi, H. Funabashi, K. Shimaoka and S. Sugiyama, “Anisotropic etching of silicon in TMAH solutions,” Sens. Actuators A Phys., vol. 34, no. 1, pp. 51-57, July 1992.

[9] I. H. Choi and K. D. Wise, “A Silicon-Thermopile-Based Infrared Sensing Array for Use in Automated Manufacturing,” IEEE Trans. on Electron Devices, vol. 33, no. 1, pp. 72-79, January 1986.

[10] K. R. Williams and R. S. Muller, “Etch rates for micromachining processing,” J. Microelectromechanical Syst., vol. 5, no. 4, pp. 256-269, December 1996.

[11] J. M. Bustillo, R. T. Howe and R. S. Muller, “Surface micromachining for microelectromechanical systems,” Proc. IEEE, vol. 86, no. 8, pp. 1552-1574, August 1998.

[12] O. Paul, D. Westberg, M. Hoernung, V. Ziebart and H. Baltes, “Sacrificial aluminum etching for CMOS microstructures,” Proc. IEEE Workshop Micro Electro Mechanical Systems MEMS’97, pp. 523-528, Japan, 26-30 January 1997.

[13] N. Shen, J. Yu and Z. Tang, “An Uncooled Infrared Microbolometer Array for Low-Cost Applications,” IEEE Photonics Technology Letters, vol. 27, no. 12, pp. 1247-1249, June 2015.

[14] V. Linder, B. D. Gates, D. Ryan, B. A. Parviz and G. M. Whitesides, “Water-Soluble Sacrificial Layers for Surface Micromachining,” small, vol.1, no. 7, pp. 730-736, June 2005.

[15] B. Wang, J. Lai, E. Zhao, H. Hu, Q. Liu and S. Chen, “Vanadium oxide microbolometer with gold black absorbing layer,” Opt. Eng., vol. 51, no. 7, 074003, July 2012.

[16] J. Bühler, F.-P. Steiner and H. Baltes, “Silicon dioxide sacrificial layer etching in surface micromachining,” J. Micromech. Microeng., vol. 7, R1, January 1997.

[17] H. Wang, X. Yi, J. Lai and Y. Li, “Fabricating Microbolometer Array on Unplanar Readout Integrated Circuit,” Int J Infrared Milli Waves, vol. 26, no. 5, pp. 751-762, April 2005.

[18] F. Hedrich, S. Billat and W. Lang, “Structuring of membrane sensors using sacrificial porous silicon,” Sens. Actuators A Phys., vol. 84, no. 3, pp. 315-323, September 2000.

[19] R. Lenggenhager, H. Baltes and T. Elbel, “Thermoelectric infrared sensors in CMOS technology,” Sens. Actuators A Phys., vol. 37, pp. 216-220, June/August 1993.

[20] N. Sharma, M. Hooda and S. K. Sharma, “Synthesis and Characterization of LPCVD Polysilicon and Silicon Nitride Thin Films for MEMS Applications,” Journal of Materials, vol. 2014, pp. 1-8, April 2014.

[21] D. Maier-Schneider, A. Köprülülü, S. Ballhausen Holm and E. Obermaier, “Elastic properties and microstructure of LPCVD polysilicon films,” J. Micromech. Microeng., vol. 6, no. 4, pp. 436-446, September 1996.

[22] M. Orpana and A. O. Korhonen, “Control of residual stress of polysilicon thin films by heavy doping in surface micromachining,” Proc. 6th Int. Conf. on Solid-State Sensors and Actuators (Transducers ’91), USA, 24-27 June 1991.

[23] P. Temple-Boyer, C. Rossi, E. Saint-Etienne and E. Scheid, “Residual stress in low pressure chemical vapor deposition SiNx films deposited from silane and ammonia,” J. Vac. Sci. Technol A, vol. 16, no. 4, pp. 2003-2007, July/August 1998.

[24] J. M. Olson, “Analysis of LPCVD process conditions for the deposition of low stress silicon nitride. Part I: preliminary LPCVD experiments,” Mater. Sci. Semicond. Process., vol. 5, no. 1, February 2002.

[25] R. Vora, I. Spies, D. Hoffmann, H. Trautner, C. Blattert and A. Dehe, “Vapor HF Etching Based Surface Micromachining Process for Fabricating a Micromechanical Sterilization Cycle Counter,” Proc. MikroSystemTechnik Congress 2021, Germany, 8-10 November 2021.

[26] N. Schneeberger, O. Paul and H. Baltes, “Spectral infrared absorption of CMOS thin film stacks,” Int. Conf. on Micro Electromechanical Systems (MEMS’99), pp. 106-111, 1999.

[27] S. Timoshenko, “Analysis of bi-metal thermostats,” J. Opt. Soc. Amer., vol. 11, no. 3, pp. 233-255, May 1925.

[28] Z.-C. Feng and H.-D. Liu, “Generalized formula for curvature radius and layer stresses caused by thermal strain in semiconductor multilayers,” J. Appl. Phys., vol. 54, no. 1, pp. 83-85, January 1983.

[29] J. M. Gere and B. J. Goodno, “Mechanics of Materials,” vol. 8, Cengage Learning, 2012.

[30] E. Garcia and N. Lobontiu, “Induced-strain multimorphs for microscale sensory actuation design,” Smart Mater. Struct., vol. 13, no. 4, pp. 725-732, August 2004.

[31] O. Paul and P. Ruther, “Material Characterization,” in CMOS-MEMS, O. Brand and G. K. Fedder, WILEY - VCH Verlag GmbH & Co. KGaA, 2005, pp. 69-135.

[32] R. W. Johnstone, D. Sameoto and M. Parameswaran, “Non-uniform residual stresses for parallel assembly of out-of-plane surface-micromachined structures,” J. Micromech. Microeng., vol. 16, no. 11, N17-N21, September 2006